

# JGR Solid Earth

## RESEARCH ARTICLE

10.1029/2021JB022503

## New Paleomagnetic Constraints on the Cretaceous Tectonic Framework of the Antarctic Peninsula

Liang Gao<sup>1,2</sup> , Junling Pei<sup>2,3</sup> , Yue Zhao<sup>1,2,3</sup>, Zhenyu Yang<sup>4</sup> , Teal R. Riley<sup>5</sup>, Xiaochun Liu<sup>2,3</sup>, Shuan-Hong Zhang<sup>2,3</sup> , and Jian-Min Liu<sup>2,3</sup>

<sup>1</sup>School of Ocean Sciences, China University of Geosciences, Beijing, China, <sup>2</sup>Key Laboratory of Paleomagnetism and Tectonic Reconstruction of Ministry of Land and Resources, Beijing, China, <sup>3</sup>Institute of Geomechanics, Chinese Academy of Geological Sciences, Beijing, China, <sup>4</sup>College of Resources, Environment and Tourism, Capital Normal University, Beijing, China, <sup>5</sup>British Antarctic Survey, Cambridge, UK

### Key Points:

- We have obtained a key mid-Cretaceous paleopole (58.1°S, 354.3°E, A<sub>95</sub> = 6.3°) from the Byers Peninsula, South Shetland Islands
- South Shetland Islands located at the Pacific margin of southern Patagonia-Fuegian Andes during the Early to mid-Cretaceous
- Consistent almost northward paleomagnetic declination support an autochthonous model for most part of the Antarctic Peninsula

### Supporting Information:

Supporting Information may be found in the online version of this article.

### Correspondence to:

J. Pei and L. Gao,  
[peijunling@gmail.com](mailto:peijunling@gmail.com);  
[lgao@live.cn](mailto:lgao@live.cn)

### Citation:

Gao, L., Pei, J., Zhao, Y., Yang, Z., Riley, T. R., Liu, X., et al. (2021). New paleomagnetic constraints on the Cretaceous tectonic framework of the Antarctic Peninsula. *Journal of Geophysical Research: Solid Earth*, 126, e2021JB022503. <https://doi.org/10.1029/2021JB022503>

Received 26 MAY 2021

Accepted 11 OCT 2021

**Abstract** Understanding the tectonic framework of the Antarctic Peninsula is hindered by a paucity of paleomagnetic data from key locations. In this study, we present paleomagnetic data from the South Shetland Islands, to the northwest of the Antarctic Peninsula, which provides valuable paleoposition constraints on the Western domain of the Antarctic Peninsula. We report a key reliable paleopole (58.1°S, 354.3°E, A<sub>95</sub> = 6.3°) from Livingston Island in the South Shetland Islands at ~102 Ma. Plate reconstruction models from the Early Cretaceous attach the South Shetland Islands to the Pacific margin of southern Patagonia-Fuegian Andes at ~140 Ma. The South Shetland Islands then experienced southward translation to its current position to the northwest of the Antarctic Peninsula following counterclockwise rotation during ~100–90 Ma. A similar counterclockwise rotation has also been identified from southern Patagonia-Fuegian Andes but is absent in the Antarctic Peninsula, suggesting a direct affinity between the South Shetland Islands and southern Patagonia-Fuegian Andes. However, the consistent, almost northward Cretaceous paleomagnetic declination in the Antarctic Peninsula, and the near-synchronous tectonic-magmatic history between the Antarctic Peninsula and the southern Patagonia-Fuegian Andes support an autochthonous continental subduction model for most of the Antarctic Peninsula.

**Plain Language Summary** In this study, we applied paleomagnetic constraints on the autochthonous continental subduction model and allochthonous terrane accretion model in the explanation of the tectonic framework of the Antarctic Peninsula. Our new data reveal a consistent counterclockwise rotation occurred both at the South Shetland Islands and southern Patagonia-Fuegian Andes during ~100–90 Ma, suggesting the affinity of these places. This is supported by the previous reported ~140 Ma plate reconstruction, which attached the South Shetland Islands to the Pacific margin of southern Patagonia-Fuegian Andes. However, the lack of significant tectonic rotation suggests that most parts of the Antarctic Peninsula were formed during the Pacific plate subduction and support an autochthonous continental subduction model.

## 1. Introduction

There is a continuing debate on the tectonic framework of the Antarctic Peninsula and its paleoposition in the Gondwana supercontinent during Cretaceous global plate reorganization (Dalziel & Elliot, 1982; Jordan et al., 2020). The following models have been proposed for the Antarctic Peninsula: an autochthonous continental subduction model (Burton-Johnson & Riley, 2015; Suárez & Pettigrew, 1976); an allochthonous terrane accretion model (Vaughan & Storey, 2000); and a para-autochthonous geophysical model in which part of the arc was formed in situ but part of it may have been exotic, even if not from a distant location (Ferraccioli et al., 2006). Plate reconstruction models are primarily based on syntheses of geological evidence, paleomagnetic and relative plate reconstruction data and comparisons with models of plate motion within the hotspot reference frame (Seton et al., 2012). However, the development of accurate solutions is hindered by the absence of marine magnetic anomalies from the Pacific Cretaceous seafloor within the Cretaceous normal polarity superchron (124–84 Ma). Therefore, the aim of this study is to address this gap by reporting new paleomagnetic data, which place important constraints on the Western domain sector in the northern Antarctic Peninsula paleoposition during the Cretaceous.

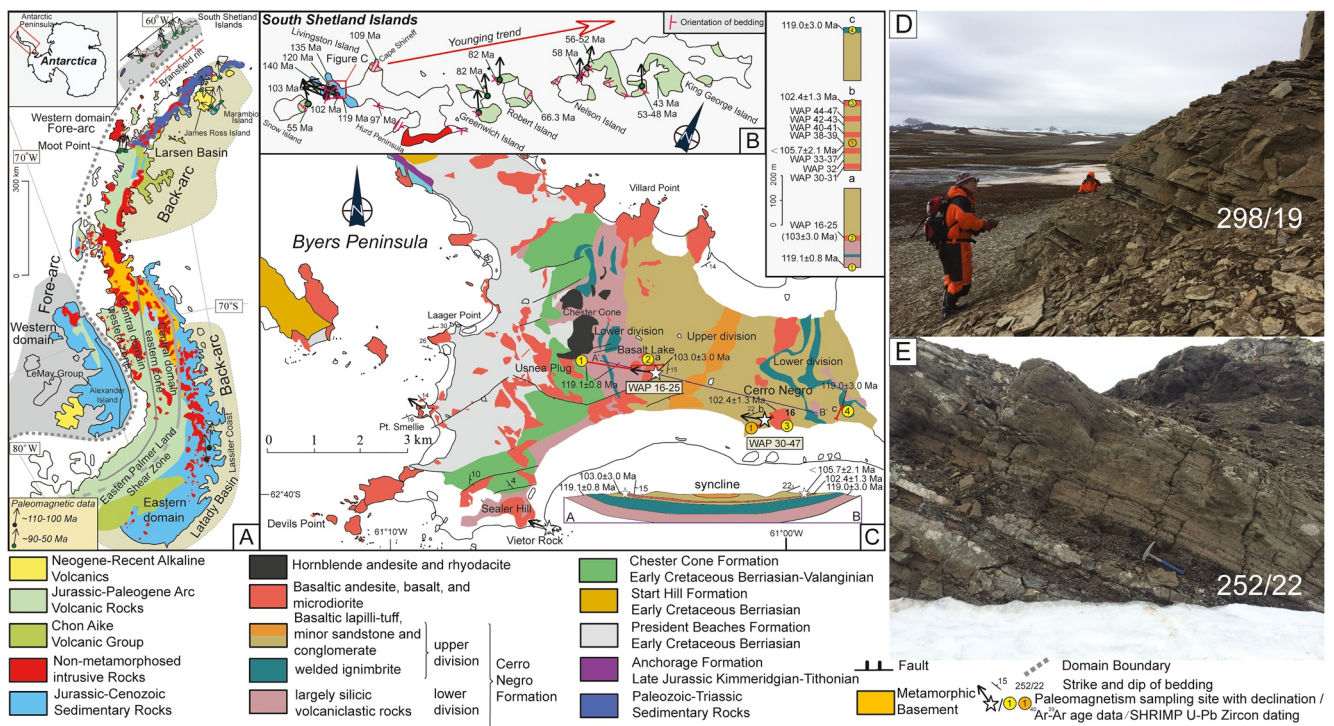


**Figure 1.** (a) Geological map of the Antarctic Peninsula, (b) South Shetland Islands, (c) Byers Peninsula (modified from Burton-Johnson & Riley, 2015; Hathway et al., 1999; Vaughan & Storey, 2000), (d and e) Photos of the sampling sites in Byers Peninsula, Livingston Island. A'—B': Cross section line.

## 2. Geological Setting and Sampling

The Antarctic Peninsula forms part of the West Antarctic collage of crustal blocks and basins (Figure 1a). The Mesozoic tectonics of the Antarctic Peninsula were initially interpreted as an Andean-type arc-trench system (Figure 1a; Smellie, 1981; Suárez & Pettigrew, 1976). The geological units were composed of fore-arc accretion-subduction complexes on the Pacific margin of the peninsula (Smellie, 1981; Suárez & Pettigrew, 1976), a magmatic arc active during ~240–20 Ma, represented by the Antarctic Peninsula batholith (Jordan et al., 2014; Leat & Riley, 2021; Leat et al., 1995; Riley et al., 2012; Zheng et al., 2018), and a thick back-arc succession of the Larsen Basin and Latady Basin (Figure 1a; Hathway & Lomas, 1998; Hunter & Cantrill, 2006). The Eastern Palmer Land Shear Zone is a major ductile to brittle-ductile shear zone that has been identified along the spine of the southern Antarctic Peninsula (Vaughan & Storey, 2000). The reverse to dextral reverse deformation is identified from breccia, mylonites and pseudotachylites in the shear zone (Vaughan & Storey, 2000). This deformation event along the shear zone was identified as the Palmer Land Event, which has been dated at  $106.9 \pm 1.1$  Ma and  $102.8 \pm 3.3$  Ma through  $^{40}\text{Ar}$ - $^{39}\text{Ar}$  dating of a syn-deformation granitic dyke from southeastern Palmer Land and of a biotite from a shear zone mylonite from eastern Palmer Land, respectively (Vaughan, Kelley, & Storey, 2002; Vaughan, Pankhurst, & Fanning, 2000). Combined with the identification of the Eastern Palmer Land Shear Zone, Vaughan and Storey (2000) separated the Antarctic Peninsula into three distinct geological terranes: the allochthonous Western domain, the allochthonous magmatic arc Central domain, and the parautochthonous Eastern domain (Vaughan & Storey, 2000) (Figure 1a). They suggested that distinct geological terranes and large-scale shear zone in the Antarctic Peninsula are comparable to the subduction-accretion complex in New Zealand, Marie Byrd Land, and south-central Chile along the proto-Pacific margin of Gondwana, where allochthonous magmatic arc terranes are in tectonic contact with parautochthonous cratonic or old mobile-belt basement through a deformation zone, similar to the Eastern Palmer Land Shear Zone (Vaughan & Storey, 2000).

The turbiditic sandstones and allochthonous oceanic basalts and sediments of the Jurassic-Cretaceous accretionary complex, such as the LeMay Group of the Alexander Island (Figure 1a; Holdsworth & Nell, 1992), and amphibolite with blueschist grade rocks of the Scotia Metamorphic Complex in the South Shetland

Islands (Figure 1a; Dalziel, 1972a; Dalziel & Elliot, 1971; Tanner et al., 1982; Trouw et al., 2000) are proposed to constitute an allochthonous Western domain (Vaughan & Storey, 2000). To the east, pre-Late Triassic marble tectonic breccia, Late Triassic K-feldspar megacrystic granitoids and quartzo-feldspathic granitoid gneisses were intruded by Jurassic-Cretaceous plutons in the Central domain (Vaughan & Storey, 2000). This domain was further suggested to be a composite magmatic arc terrane, separated into the allochthonous Central domain western zone and the parautochthonous Central domain eastern zone based on the distinct geologic, petrologic, isotopic and geophysical characteristic (Ferraccioli et al., 2006). The latest extension-controlled Jurassic to Early Cretaceous (141–127 Ma) adakitic plutons were emplaced in the Triassic and Jurassic gneissic and plutonic rocks of Central domain western zone (Figure 1a; Ferraccioli et al., 2006; Vaughan & Storey, 2000). This adakitic rocks resemble mantle-derived magmas of oceanic island arcs, with some pre-existing continental imprint involved in magma generation (Ferraccioli et al., 2006; Wareham et al., 1997). The ilmenite-rich and more felsic batholith (compared to the Central domain western zone) of the Central domain eastern zone developed along the Eastern domain, with island arc magmatism emplacement of tholeiitic dykes at ~120–107 Ma (Ferraccioli et al., 2006). The final suturing between the Central domain western zone and Central domain eastern zone was ascribed to cause the transpressional events at Eastern Palmer Land Shear Zone (Ferraccioli et al., 2006). Along the convergent margin of the Gondwana supercontinent (Jordan et al., 2017), the Eastern domain was proposed to be separated from the Central domain eastern zone by the Eastern Palmer Land Shear Zone (Figure 1a; Ferraccioli et al., 2006; Vaughan & Storey, 2000). Late Paleozoic basement was covered by the Mesozoic sedimentary basins in the Eastern domain, including silicic volcanic rocks related to the breakup of Gondwana, and the marine clastic sequences of the Latady Basin (Hunter & Cantrill, 2006). However, recent reinterpreted geological evidence gives more support to the autochthonous continental subduction model (Burton-Johnson & Riley, 2015). They cite evidence that include the similar Early Palaeozoic basements and deep crustal structures, and the stratigraphic and geochronological correlation of different sequences between the autochthonous and previously suggested allochthonous terranes among others (Burton-Johnson & Riley, 2015). Jurassic to Late Pleistocene volcanic-sedimentary rocks are widely distributed in the South Shetland Islands, which are separated from the Antarctic Peninsula by the Bransfield rift since the Pliocene (Figure 1b; Haase et al., 2012; Smellie & Hole, 2021). The age of the magmatism has been constrained at ~140–20 Ma with a decreasing trend from southwestern Livingston Island to northeastern King George Island (Figure 1b; Haase et al., 2012; Leat & Riley, 2021; Smellie et al., 1984). The continuous magmatic events exclude large-scale relative plate motion among these islands because large-scale relative motion would disturb the regular distributed magmatism. On Livingston Island, there are three main stratigraphic units, the Miers Bluff Formation, the Byers Group, and the Coppermine Formation (Smellie et al., 1984). The name Miers Bluff Formation was introduced by Dalziel (1972b). This Formation crops out at the Hurd Peninsula, Livingston Island, which mainly consists of turbiditic sandstones, mudstones, conglomerates and sedimentary breccias (Figure 1b; Dalziel, 1972b; Hervé, Faúndez, et al., 2006; Hervé, Miller, & Pimpirev, 2006). The age of this succession was assigned to the Late Jurassic-Late Cretaceous based on SHRIMP U-Pb zircon age dating and calcareous nannoplankton fossils (Hervé, Faúndez, et al., 2006; Pimpirev et al., 2002, 2006). This formation has been proposed to be deposited in a multiple source, gravel-rich, deep-sea ramp system and has undergone significant deformation and was emplaced in a strike-slip fault setting (Muñoz et al., 1992). Byers Peninsula is located in the western part of Livingston Island, South Shetland Islands (Figure 1a; Hobbs, 1968). The Byers Group is Late Jurassic to Early Cretaceous in age and constitutes the dominant exposed succession in Byers Peninsula, it was emplaced in a deep marine to continental fore-arc basin setting (Figure 1c; Bastias et al., 2019; Hathway & Lomas, 1998; Smellie et al., 1980). This Group was divided into the following five formations: Anchor-age (?Kimmeridgian-Tithonian), President Beaches (Berriasian), Start Hill (late Berriasian), Chester Cone (?latest Berriasian-mid Valanginian), and Cerro Negro (Aptian) (Hathway & Lomas, 1998) (Figure 1c). The age of these formations has been determined by isotope geochronology and palynology (Hathway & Lomas, 1998; Smellie et al., 1980). The Cerro Negro Formation has been sampled for paleomagnetic analysis as part of this study (Figures 1c–1e). This formation includes a lower interval of welded and non-welded ignimbrites, intercalated with subordinate reworked silicic pyroclastic and epiclastic strata, and a poorly sorted upper division which includes basalt, basaltic lapilli-tuffs, tuffaceous breccias, sandstone, and mudstone (Figure 1b; Hathway & Lomas, 1998).

New paleomagnetic samples were collected from both basaltic lava flows and bedded tuffs from the upper part of the Cerro Negro Formation across 28 sites on Byers Peninsula (Figure 1c). The Cerro Negro Formation is interpreted to be tilted but not folded (Smellie et al., 1980). However, both our field work and the geological map (Hathway et al., 1999) suggest a possible slight syncline in this formation (Figure 1c). The approximate NW-SE to NE-SW folding axis is similar to the NW-SE-oriented large-scale folds exposed at Cape Shirreff (Pallàs et al., 1999), which is only ~24 km away from the Byers Peninsula (Figure 1c). Two sections on both limbs of the syncline were sampled (Figure 1c). One section was located on the western limb near the basalt lake area (WAP 16–25; GPS: 62.65°S, 61.07°W); the basalt yielded an age of  $103.0 \pm 3.0$  Ma using whole rock  $^{40}\text{Ar}/^{39}\text{Ar}$  dating (Gracanin, 1983), and the nearby welded silicic ignimbrite clast in the lower part of the formation yielded an age of  $119.1 \pm 0.8$  Ma from  $^{40}\text{Ar}/^{39}\text{Ar}$  dating of plagioclase (Hathway et al., 1999). The other section was sampled at sites close to the Cerro Negro (WAP 30–47; GPS: 62.66°S, 61.00°W) (Figure 1c). This section is located on the east limb of the syncline, and whole rock  $^{40}\text{Ar}/^{39}\text{Ar}$  dating of basalt yielded an age of  $102.4 \pm 1.3$  Ma (Haase et al., 2012). To the east, the lower part of the formation formed at  $119.0 \pm 3.0$  Ma based on  $^{40}\text{Ar}/^{39}\text{Ar}$  dating of silicic ignimbrite plagioclase (Figure 1c; Hathway et al., 1999).

All samples were located with a handheld GPS and oriented with a magnetic compass in the field. We measured the strike and dip of the lava flows and tuffs at the lithologic boundaries (Figures 1d and 1e). Samples were collected from 23 lava flows with average thickness of ~1.5 m, and 5 sites from tuffs with the average thickness of ~2 m. All samples were collected away from the faults to avoid any influence from the local deformation. The magnetic compass did not show any obvious deviation when it was gradually moved close to the basalt. Meanwhile, solar compass was used by previous studies, which showed insignificant magnetic variation ( $\leq 3^\circ$ ) compared to the predicted magnetic direction (Grunow, 1993). A platform drill in the laboratory was used to take standard paleomagnetic specimens (150 core specimens). The twelfth Generation International Geomagnetic Reference Field was used to correct for the present-day declination ( $D = 13.0^\circ$ ) (Thébault et al., 2015).

### 3. Methods

#### 3.1. SHRIMP U-Pb Zircon Dating

The fresh tuff samples were crushed, and heavy liquids and a Frantz magnetic separator were used to extract the zircons. Then, the zircons were handpicked, mounted in epoxy resin, and polished to expose the center of the grains. To better identify the morphology and internal textures of these grains and help us to choose potential target site without influence from fracture and inclusion for later U–Th–Pb analysis of the grains, we used an optical microscope to take photographs. Meanwhile, a scanning electron microprobe (SEM) was applied to take cathodoluminescence (CL) images. In order to obtain the youngest age, the concentric oscillatory zoning in the magmatic zircon was set as our first choice to perform measurement. For those with small concentric oscillatory zoning, we prefer to analyse place with the same color as concentric oscillatory zoning. We set the target point in the core, when analysing the metamorphic zircon.

We undertook the isotope analyses on a SHRIMP II ion microprobe at the Beijing SHRIMP Center, Institute of Geology, Chinese Academy of Geological Sciences. Detailed analytical procedures have been described in Compston et al. (1992). Analytical mass resolution was 5000 (1% definition). The intensity of the primary ion beam was 5–8 nA with the beam size of 25–30  $\mu\text{m}$ . Prior to analysis, we rastered each site with 120–200 s, followed with five scans through the mass stations. The standard TEM ( $^{206}\text{Pb}/^{238}\text{U}$  age = 416.8 Ma) was used to calibrate the isotope ratios. The data were processed with the SQUID and ISOPLOT programs, and the measured  $^{204}\text{Pb}$  was used to correct the common lead (Ludwig, 2003). The uncertainties for individual analyses are applied at the  $1\sigma$  confidence, and 95% confidence level for pooled ages. The reported ages are primarily determined from the  $^{206}\text{Pb}/^{238}\text{U}$  ratios.

#### 3.2. Paleomagnetism and Rock Magnetism

The specimens were progressively demagnetized using thermal (99 specimens) or alternating field (AF) (42 specimens) demagnetization with 9–16 steps, up to ~610°C or 180 mT. The remaining nine specimens were not used in further demagnetization process, because some samples are too small or have an irregular

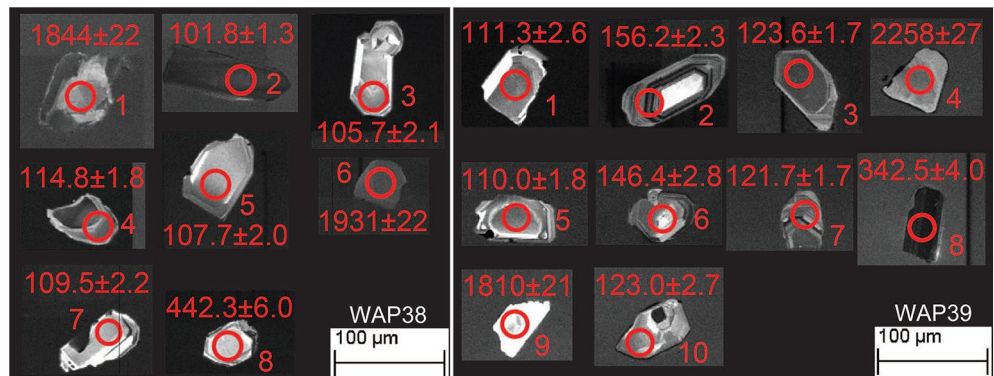


**Figure 2.** Cathodoluminescence images of zircon crystals with the analyzed spots and ages.

shape, while others exploded into small fragments after heating to  $\sim 400$  °C. After each step, the remanent magnetization was measured with an AGICO JR6 spinner magnetometer in a magnetically shielded room with a background magnetization of  $<10$  nT. Principal components analysis (Kirschvink, 1980) was used to calculate the characteristic component directions. Fisherian statistics was applied to calculate the site-mean direction (Fisher, 1953). All data were processed with the KIRSCH and PMSTAT software packages of Enkin (1994) and “PaleoMac” software (Cogné, 2003).

Before demagnetization, the anisotropy of magnetic susceptibility (AMS) was measured for eight tuff specimens using a KLY-3 Kappabridge. To further identify the magnetic carriers in these specimens, we conducted systematic rock magnetic experiments, including measurement of hysteresis loops, first order reversal curves (FORCs), and isothermal remanent magnetization (IRM) acquisition, which were performed on representative specimens with a peak field of 0.45 T. We obtained the saturation magnetization ( $M_s$ ), saturation remanent magnetization ( $M_{rs}$ ), coercive force ( $B_c$ ), and remanent coercivity ( $B_{cr}$ ) values from the hysteresis loops and FORCs using an alternating gradient magnetometer (MicroMag Model 3900, Princeton Measurements Inc.) at room temperature. All data were corrected for paramagnetic contributions prior to data processing, which was conducted with FORCinel 1.18 software (Harrison & Feinberg, 2008).

To determine the primary thermoremanent (TRM) characteristics of the basalt specimens, we selected representative specimens for natural remanent magnetization/isothermal remanent magnetization (NRM/IRM) demagnetization experiments (Cisowski et al., 1990). The AF demagnetization spectra of both NRM and IRM were compared using equivalent fields. These experiments were conducted at the Key Laboratory of Paleomagnetism and Tectonic Reconstruction of the Ministry of Land and Resources, Beijing and Paleomagnetism and the Environmental Magnetism Laboratory of the China University of Geosciences, Beijing.

Our plate reconstructions are based on both the paleomagnetic data and geological evidence. The paleomagnetic declination and inclination were used to constrain the plate rotation and latitude translation. The geological records were also used to constrain the opening and closing of Rocas Verdes basin and the tectonic evolution of the Antarctic Peninsula. We used the GPlates software to do the plate reconstruction ([www.gplates.org](http://www.gplates.org); Boyden et al., 2011; Müller et al., 2018). The best-fit small circle of paleopoles and the position of Euler poles were calculated with “PaleoMac” software (Cogné, 2003). Detailed calculation processes of Euler poles can be found in the appendix of Butler (1998).

## 4. Results and Data Analysis

### 4.1. SHRIMP U-Pb Zircon Dating

Eighteen zircon grains were analyzed from two tuff samples, and the results are listed in Table S1 in Supporting Information S1. These two samples were collected from the same location of Cerro Negro Formation; therefore, we analyzed all the data together. The zircon grain size is ca. 50–100  $\mu\text{m}$  in length, and the length/width ratios range from equant to about 3:1 (Figure 2). We identified three groups of ages, which are 1810–2258 Ma (4 grains), 342.5–442.5 Ma (2 grains), and 101.8–156.2 Ma (12 grains). The younger ages

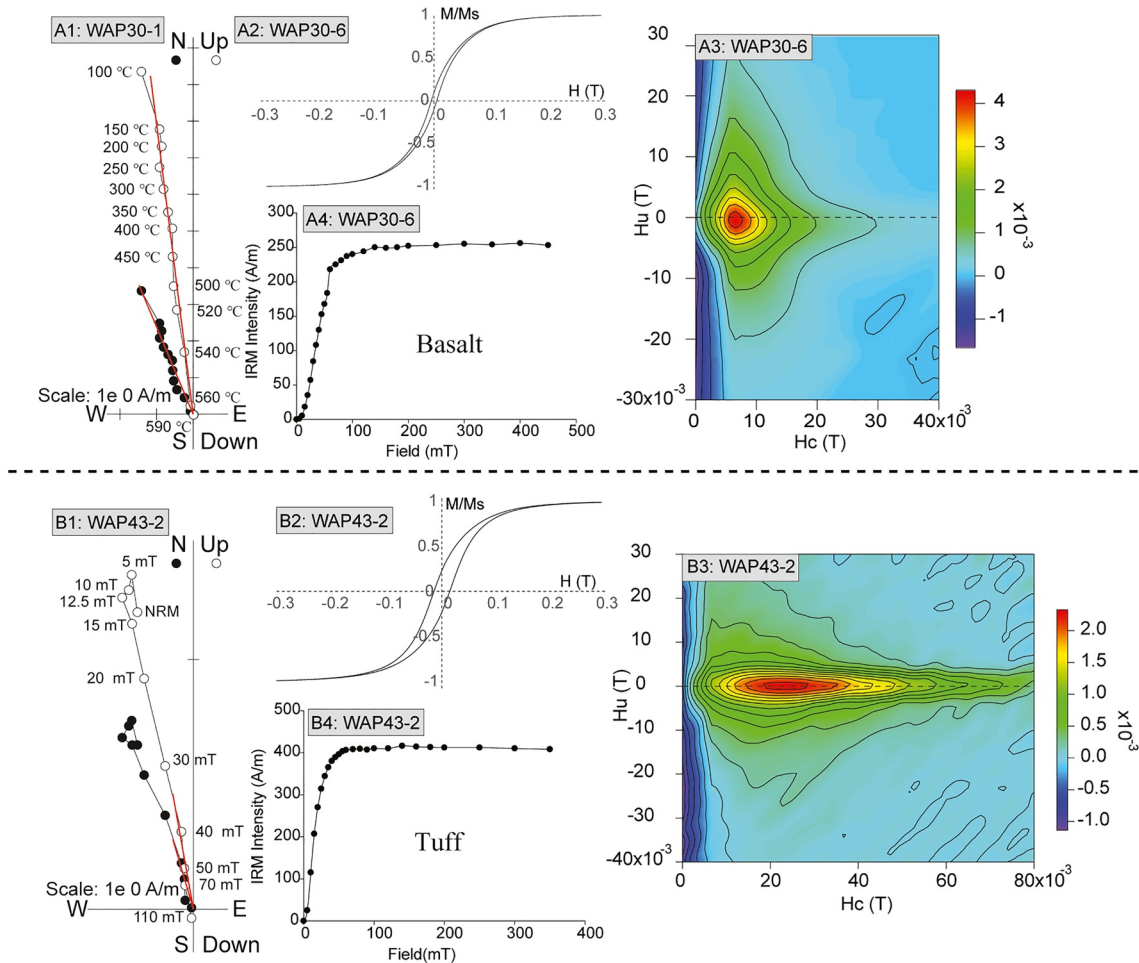


**Figure 3.** (a1, b1) Representative Zijderveld diagrams of the thermal and AF demagnetization of NRM; (a2, b2) Hysteresis loops; (a3, b3) FORC diagram for representative specimens from Byers Peninsula; (a4, b4) Isothermal remanent magnetization acquisition curves.  $H_c$  and  $H_c$ : Coercive force.

(101.8–156.2 Ma) are mainly from the euhedral-subhedral zircon grains, exhibiting concentric oscillatory zoning, strongly suggesting a magmatic origin. Spots WAP 38-1 ( $1844 \pm 22$  Ma), 38-6 ( $1931 \pm 22$  Ma), and 39-4 ( $2258 \pm 27$  Ma) have lower Th/U values ( $<0.4$ ), with no oscillatory zoning indicating that they may be metamorphic in origin (Table S1 in Supporting Information S1). Zircon analyses of WAP 38-2 ( $101.8 \pm 1.3$  Ma) and WAP 39-8 ( $342.5 \pm 4.0$  Ma) exhibit higher contents of Th and U than normal values, indicating that these grains might be modified by hydrothermal alteration (Figure 2; Table S1 in Supporting Information S1). Thus, these grains were excluded from the data analyses. The youngest grains ( $\sim 123$ – $105$  Ma) correspond well with the Cretaceous magmatism flare-up episodes at  $\sim 125$  Ma, 115 Ma, and 105 Ma in the Antarctic Peninsula (Riley et al., 2018, 2019). The youngest age ( $105.7 \pm 2.1$  Ma) is consistent with previous  $^{40}\text{Ar}/^{39}\text{Ar}$  dating results on basaltic units ( $102.4 \pm 1.3$  Ma– $103.0 \pm 3.0$  Ma; Hathway et al., 1999; Haase et al., 2012), and it is likely that the tuff unit was deposited soon after this.

#### 4.2. Paleomagnetism and Rock Magnetism

The natural remanent magnetization intensities range from 0.057 to 10.99 A/m for the basalt and from 0.084 to 1.75 A/m for the tuff. One or two components were isolated during the thermal and AF demagnetization (Figure 3). The magnetization direction obtained from the thermal demagnetization technique is almost identical to the direction isolated from the AF demagnetization technique (Figures 3a1 and 3b1). A low-temperature component or low-coercivity component was isolated around  $200^\circ\text{C}$  or 12.5 mT, and subsequent to its removal, a high-temperature or high-coercivity component was revealed at  $\sim 590^\circ\text{C}$  or

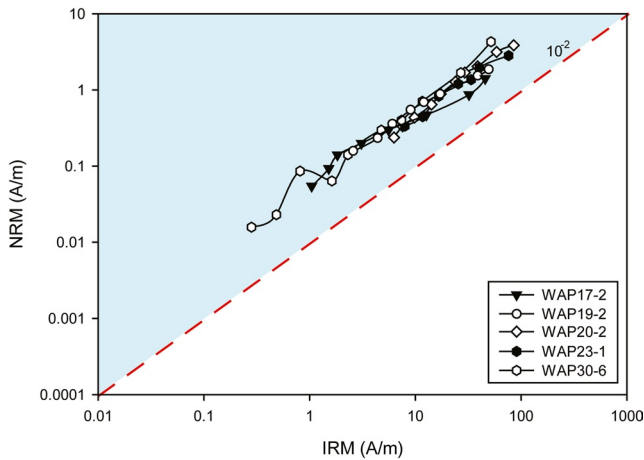


**Figure 4.** Results of natural remanent magnetization/isothermal remanent magnetization analysis. Note that values exceed  $10^{-2}$  for five representative basalt specimens, indicating that they carry the original thermoremanent.

$\sim 110$  mT (Figure 3), indicating the presence of magnetite. The hysteresis loops closed below 200 mT and exhibited a less divergent contour pattern in FORC diagrams, with a peak  $H_c$  value at  $\sim 20$  mT, indicating the dominance of single domain magnetite (Figures 3a2, 3b2, 3a3, and 3b3; Dunlop & Özdemir, 2001; Roberts et al., 2000). The IRM acquisition curves support the conclusion that magnetite is the dominant magnetic carrier (Figures 3a4 and 3b4). The NRM/IRM values for basalt specimens exceed  $10^{-2}$ , also indicating that magnetite carries the primary TRM (Cisowski et al., 1990) (Figure 4).

We discarded paleopole (WAP42; eight specimens) that was away from the averaged paleomagnetic pole by  $>45^\circ$  (Table 1). Reliable high-temperature or high-coercivity components were isolated from 133 samples of 21 sites (Figures 5a and 5b). They yielded mostly normal and one reverse-polarity site-mean directions, giving an in situ site-mean direction of  $D_g = 330.8^\circ$ ,  $I_g = -70.8^\circ$ ,  $k_g = 23.5$ ,  $\alpha_{95} = 6.7^\circ$  and  $D_s = 286.1^\circ$ ,  $I_s = -75.5^\circ$ ,  $k_s = 82.7$ ,  $\alpha_{95} = 3.5^\circ$  after tilt correction (Figures 5a and 5b; Tables 1 and S2 in Supporting Information S1). Remanence of WAP 33 (five specimens) with reverse-polarity may have been acquired during the short reverse-polarity zone in Albian (M-3r;  $\sim 103$  Ma; Ogg, 2020), which is consistent with the age data. The positive fold test result and

100% optimum unfolding result during syn-tilting Fisher analysis indicate that the magnetization may have been acquired prior to the folding event (Figure 5d; Enkin, 2003; Watson & Enkin, 1993). The directions of the maximum ( $k_1$ ), intermediate ( $k_2$ ), and minimum ( $k_3$ ) ellipsoid axes are shown on a stereonet projection (Figures 5e and 5f). AMS results of bedded tuffs show that the  $k_3$  axes became generally vertical after tilt correction, and the  $k_1$  and  $k_2$  axes are separated in the horizontal plane. This is a typical depositional magnetic fabric without significant deformation influence (Hrouda, 1982) and support the use of tilt-corrected paleomagnetic direction (Figures 5e and 5f).

To ensure that paleosecular variation (PSV) of the basalt specimens was fully averaged out, we calculated their PSV (Deenen et al., 2011). The  $A_{95} = 3.14^\circ$  calculated from the specimen-level paleopole is located within the range of  $A_{95 \max} = 4.40^\circ$  and  $A_{95 \min} = 1.87^\circ$  ( $N = 104$ ). Therefore, the basalt specimens reliably record the geomagnetic field. In addition, the tuff specimens carried a Detrital Remanent Magnetization, which has almost the same direction as that of the basalt specimens (Table S2 in Supporting Information S1), confirming that the PSV of the basalt specimens has been fully averaged. Although it is difficult to determine the folding time, combining the primary TRM character of the basalt specimens, the positive folding test result, and the high value of optimum grouping during the syn-tilting Fisher analysis, leads us to conclude these rocks mostly carried a characteristic remanent magnetization (ChRM). Meanwhile, both the in situ ( $73.3^\circ\text{S}$ ,  $42.4^\circ\text{E}$ ,  $A_{95} = 10.9^\circ$ ) and tilt corrected ( $58.1^\circ\text{S}$ ,  $354.3^\circ\text{E}$ ,  $A_{95} = 6.3^\circ$ ) paleopoles are far away from the Late Cretaceous-Eocene Antarctic Peninsula and South Shetland Islands paleopoles (Figure 5c; Gao et al., 2018; Milanese et al., 2019; Poblete et al., 2011; Tobin et al., 2012), which further excluded the possibility of remagnetization.

## 5. Discussion

### 5.1. Cretaceous-Early Eocene Paleomagnetic Data From the South Shetland Islands and Antarctic Peninsula

Cretaceous-early Eocene paleomagnetic data have been reported from different areas of the South Shetland Islands and Antarctic Peninsula, which were used in plate reconstructions of different domains of the Antarctic Peninsula (Bakhmutov & Shpyra, 2011; Blundell, 1962; Dalziel et al., 1973; Gao et al., 2018; Grunow, 1993; Kellogg & Reynolds, 1978, 1989; Milanese et al., 2019, 2020; Poblete et al., 2011; Watts et al., 1984). Among these studies, data from sedimentary rocks and lava flows of Livingston Island have a similar age ( $\sim 140$  Ma) but different mean directions (Figure 1c; Grunow, 1993). The mean direction of lava flows ( $D_s = 320.1^\circ$ ,  $I_s = -62.2^\circ$  after tilt correction) passed both fold test and reversal test and differ from other directions after  $\sim 140$  Ma, therefore, this direction is considered reliable. The geomagnetic polarity

**Table 1**

Site-Mean Directions Used in the Calculation of ~102 Ma Paleopoles of the Byers Peninsula, Livingston Island, South Shetland Islands

Site name	n	In situ	Tilt corrected	$k_s$	$\alpha_{95}$ (°)	Bedding		Paleopole	
		$D$ (°) $I$ (°)	$D$ (°) $I$ (°)			Strike (°)	Dip angle (°)	Lat. (°S)	Long. (°E) $A_{95}$ (°)
Byers Peninsula-Basalt lake area (GPS: 62.65°S, 61.07°W)									
WAP 16	4	148.7–81.7	241.1–77.9	999.9	2.4	5.0	15.0	46.8	329.2 4.4
WAP 17-18	6	27.1–85.7	291.8–76.0	103.8	6.6	5.0	15.0	60.6	356.4 11.7
WAP 19-20	6	180.4–89.1	271.6–75.0	60.4	8.7	5.0	15.0	52.1	349.1 15.2
WAP 21	5	18.1–82.1	305.8–74.7	304.3	4.4	5.0	15.0	65.3	7.4 7.6
WAP 22	4	30.4–88.7	279.6–75.5	999.9	2.4	5.0	15.0	55.5	352.0 4.2
WAP 23	4	68.8–78.3	323.8–83.2	302.3	5.3	5.0	15.0	71.8	325.0 10.3
WAP 24-25	9	43.2–79.5	319.7–78.2	78.7	5.8	5.0	15.0	72.7	355.8 10.6
Mean	7	59.2–85.4	288.4–78.4	155.8	4.9			61.4	347.3 9.1
Byers Peninsula-Cerro Negro area (GPS: 62.66°S, 61.00°W)									
WAP 30	6	329.3–74.2	189.9–82.6	270.6	4.1	252.0	22.0	48.2	302.7 7.9
WAP 31	5	319.6–57.6	287.0–75.5	343.1	4.1	252.0	22.0	58.3	355.7 7.2
WAP 32	9	317.9–53.1	292.4–71.3	999.9	0.9	252.0	22.0	56.5	8.8 1.5
WAP 33	5	122.4 77.4	15.7 75.4	678.9	2.9	252.0	22.0	35.7	307.9 5.1
WAP 34-36	9	319.0–60.2	288.2–70.3	112.7	4.9	252.0	22.0/275.0	16.0	53.7 8.0 7.9
WAP 37	8	312.1–55.7	284.1–64.7	999.9	1.4	269.0	18.0	46.2	13.5 2.0
WAP 38	4	325.4–65.3	280.9–67.1	999.9	2.4	298.0	19.0	47.3	8.1 3.6
WAP 39	8	354.2–65.4	305.5–76.5	111.5	5.3	298.0	19.0	66.4	0.6 9.5
WAP 40	7	328.9–57.6	300.6–66.0	299.9	3.5	286.0	17.0	55.0	24.8 5.2
WAP 41	9	331.7–56.2	293.6–74.2	491.8	2.3	268.0	24.0	59.7	2.6 4.0
WAP 42*	8	27.2–25.2	32.2–31.0	58.3	7.3	241.0	11.0	38.9	160.0 6.1
WAP 43	8	341.7–57.0	317.0–69.0	601.5	2.3	286.0	17.0	65.4	33.3 3.6
WAP 44-45	6	354.0–59.5	275.0–75.0	89.3	7.1	293.0	32.0	53.3	351.0 12.4
WAP 46	5	309.0–53.0	279.2–68.4	306.7	4.4	293.0	32.0	47.9	5.1 6.8
WAP 47	6	318.5–55.5	289.4–73.5	291.8	3.9	293.0	32.0	57.4	2.0 6.6
Mean	14	326.0–61.3	285.2–74.0	68.7	4.8			56.3	357.4 8.6
Mean (All)	$N = 21$	330.8–70.8	286.1–75.5	82.7	3.5			58.1	354.3 6.3

Note. Paleopole with “\*” was not used because it was away from the averaged paleomagnetic pole by >45°.

changed frequently during the Jurassic. Samples from lava flows have dual polarity, but those from the sedimentary rocks record only normal polarity ( $D_s = 24.5^\circ$ ,  $I_s = -66.9^\circ$ ). This indicates that the sedimentary rocks are most likely remagnetized (Grunow, 1993). This remagnetization event may have occurred during the Late Cretaceous, as the paleopoles from these data are close to the widespread ~90 Ma remagnetized paleopole from the northern Antarctic Peninsula (Poblete et al., 2011).

In addition, data from Vietor Rock of Livingston Island were used to calculate the ~107–108 Ma paleopole (Figure 1; Gao et al., 2018; Grunow, 1993; Watts et al., 1984); the in situ site-mean direction for Vietor Rock is  $D_g = 27.0^\circ$ ,  $I_g = -73.0^\circ$ ,  $k_g = 111.0$ , and  $\alpha_{95} = 11.8^\circ$  (Grunow, 1993). This direction differs from the tilt-corrected site-mean direction of the Cerro Negro Formation. The discrepancy may be caused by the tilting of the strata considering the very similar depositional age and primary magnetization characteristics. The tilt-corrected site-mean direction for Vietor Rock is  $D_s = 298.1^\circ$ ,  $I_s = -79.4^\circ$ ,  $k_s = 112.0$ , and  $\alpha_{95} = 11.7^\circ$  (Grunow, 1993). This direction is close to the tilt-corrected site-mean direction of the Cerro Negro Formation from this study (Figure 5g;  $D_s = 286.1^\circ$ ,  $I_s = -75.5^\circ$ ,  $k_s = 82.7$ ,  $\alpha_{95} = 3.5^\circ$ ). Therefore, the similar tilt-corrected site-mean directions from Vietor Rock and Cerro Negro Formation favor the use of tilt-corrected

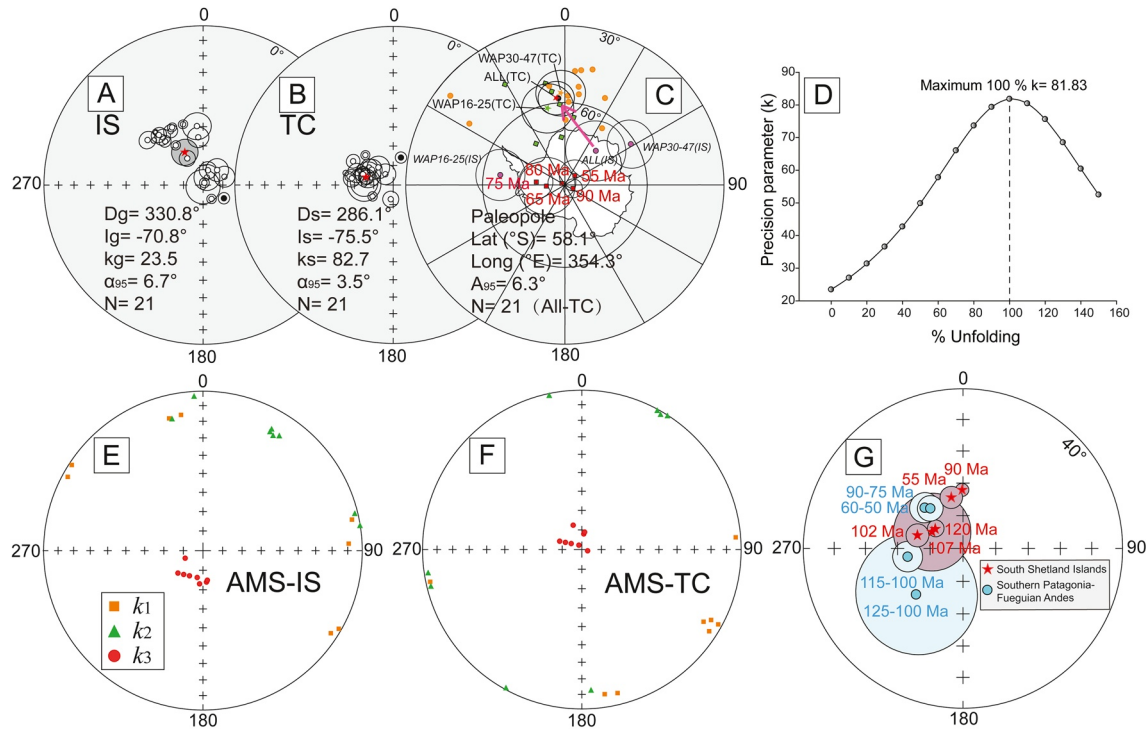


**Figure 5.** (a and b) Equal-area projections for the site-mean direction of the high-temperature and high-coercivity components, before (IS) and after (TC) tilt correction. Solid (open) symbols denote lower (upper) hemispheres. Red stars represent the average direction and the shaded circles are the 95% confidence circles; (c) Equal-area projections for the paleopoles from this study and previous studies (Gao et al., 2018; Milanese et al., 2019; Poblete et al., 2011; Tobin et al., 2012); (d) Syn-tilting Fisher analyses show that the optimum grouping of high-temperature and high-coercivity components occurs at 100% unfolding, supporting a pre-folding origin of the magnetization; (e, f) Stereonet projection of AMS before and after tilt correction; (g) Equal-area projection for site-mean direction of the South Shetland Islands, Antarctic Peninsula and southern Patagonia-Fuegian Andes.

paleomagnetic data of Vietor Rock. The site-mean direction of upper part of the Cerro Negro Formation is close to the almost flat lower part of this formation at  $\sim 120$  Ma ( $D_s = 304.3^\circ$ ,  $I_s = -73.2^\circ$ ,  $k_s = 159.1$ ,  $\alpha_{95} = 4.2^\circ$ ) (Figure 5g; Gao et al., 2018). In contrast, Cretaceous paleomagnetic data ( $\sim 106$  Ma) from Moot Point of the Central domain (western zone) and the Lassiter Coast of the Eastern domain ( $\sim 95$ – $110$  Ma) show a consistent, almost northward paleomagnetic declination (Figure 1a; Bakhmutov & Shpyra, 2011; Grunow, 1993; Kellogg & Rowley, 1989). The overlapping Late Cretaceous and Paleocene-Eocene paleopoles of South Shetland Islands and the Antarctic Peninsula (90 Ma and 55 Ma; western part of the northern Antarctic Peninsula; Grunow, 1993; Gao et al., 2018; Poblete et al., 2011; Watts et al., 1984), James Ross Island (80 Ma and 75 Ma; eastern part of the northern Antarctic Peninsula; Milanese et al., 2019), and Marambio Island (65 Ma; eastern part of the northern Antarctic Peninsula; Tobin et al., 2012) support the absence of interior relative plate rotation between the South Shetland Islands and the Antarctic Peninsula since  $\sim 90$  Ma (Figure 5c). Therefore, a new summarized paleopole at  $\sim 90$  Ma for the South Shetland Islands and Antarctic Peninsula from Poblete et al. (2011) ( $113.0^\circ\text{E}$ ,  $86.8^\circ\text{S}$ ,  $A_{95} = 3.4$ ) is used in the Late Cretaceous plate reconstruction and overlaps with the previously reported  $\sim 90$  Ma paleopole ( $152.0^\circ\text{E}$ ,  $86.0^\circ\text{S}$ ,  $A_{95} = 7.5$ ; Grunow, 1993). This represents counterclockwise rotation that occurred between Livingston Island and the Central domain and the Eastern domain of the Antarctic Peninsula during  $\sim 100$ – $90$  Ma.

## 5.2. Tectonic Framework in the Antarctic Peninsula

The combination of plate reconstructions and geological evidence provides spatio-temporal control on the tectonic history of different domains of the Antarctic Peninsula during the Cretaceous (Figures 6 and 7). We use our newly obtained paleopole at  $\sim 102$  Ma, and the previously reported  $\sim 140$  Ma paleopole (Grunow, 1993),  $\sim 90$  Ma paleopole (Poblete et al., 2011) to reconstruct the paleopositions of the South Shetland Islands (Figure 6). We also used the well-constrained paleopoles from South America (Beck Jr, 1999;

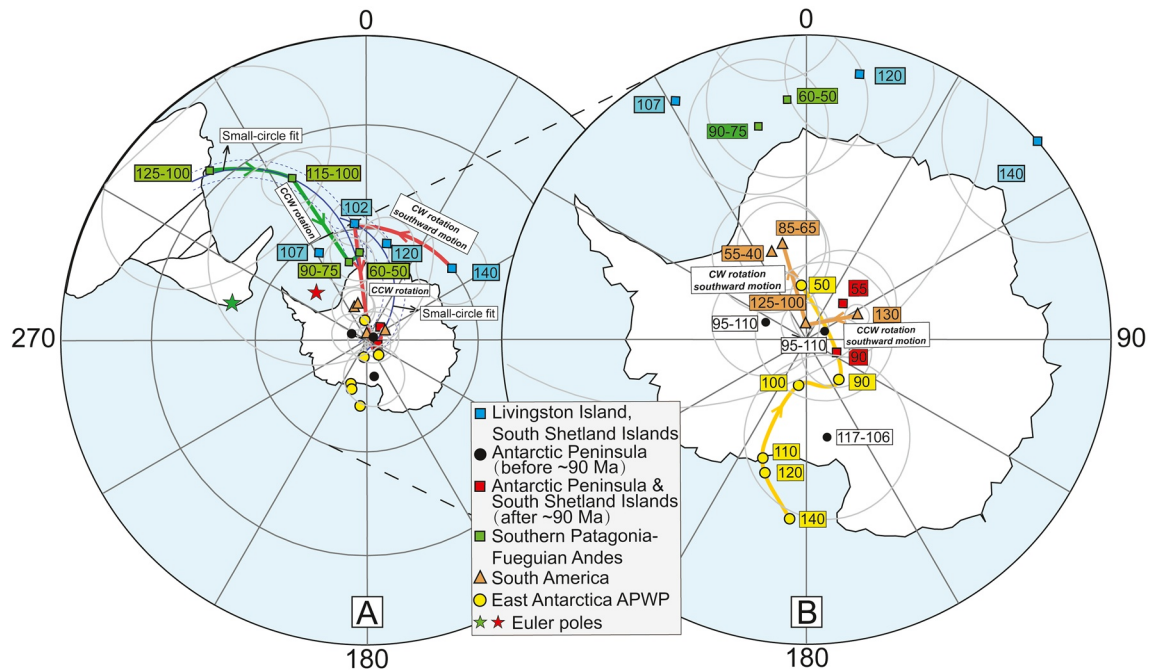


**Figure 6.** Equal-area projection for Cretaceous-Cenozoic paleopoles of the South Shetland Islands, Antarctic Peninsula, southern Patagonia-Fuegian Andes and South America. Both the South Shetland Islands and southern Patagonia-Fuegian Andes show small-scale plate motion at ~120–100 Ma, followed by a change to rapid paleopole migration at ~100–90 Ma. This supports a close relationship between these places. The South Shetland Islands experienced a counterclockwise change with the rotation pole located in the Weddell Sea, and counterclockwise rotation of the southern Patagonia-Fuegian Andes occurred around the northern Fuegian Andes.

Somoza, 2007; Somoza & Zaffarana, 2008), southern Patagonia-Fuegian Andes (SPFA) (Poblete et al., 2016), and the Antarctic Peninsula (Torsvik et al., 2012) to reconstruct the paleoposition of these locations during the Cretaceous (Figure 6; Table 2).

Our paleomagnetic reconstruction demonstrates the attachment of Livingston Island to the SPFA at ~140 Ma and was adjacent to the post-Early Permian to pre-Early Cretaceous Duque de York Complex of the SPFA (Figure 7a). The Duque de York Complex consists predominantly of turbidites, which are older than the Miers Bluff Formation of Livingston Island, and crop out along the Pacific margin of the Patagonian Batholith (Hervé, Miller, & Pimpirev, 2006). The similarities in provenance between the Duque de York Complex and the Miers Bluff Formation, as indicated by the U-Pb detrital zircon age patterns support the close affinity between these successions (Figure 7a; Barbeau et al., 2010; Castillo et al., 2016; Hervé, Faúndez, et al., 2006; Hervé, Miller, & Pimpirev, 2006). Although there is no direct coeval counterpart for the Miers Bluff Formation identified from the Pacific margin of Patagonia and the Antarctic Peninsula/South Shetland Islands, rocks with a similar age as the Miers Bluff Formation are well represented in the Austral Basin of South America (Figure 7a; Hervé, Faúndez, et al., 2006; Hervé, Miller, & Pimpirev, 2006). Therefore, it is proposed that the Miers Bluff Formation was deposited under a complete erosion of Jurassic and Cretaceous sedimentary rocks from the western Patagonian Andes (Hervé, Miller, & Pimpirev, 2006), which is consistent with the paleomagnetic reconstruction (Figure 7a).

The lithospheric rifting and depositional process of both the Rocas Verdes Basin and Larsen Basin (Norden-skjöld Formation) developed in the interval ~150–140 Ma, coincident with the emplacement of syenogranite and alkali granites (Bastias, 2020; Dalziel et al., 1974; Guillot, 2016; Hathway, 2000; Hervé, Miller, & Pimpirev, 2006; Hervé et al., 2007). This demonstrates a close spatio-temporal relationship between the Antarctic Peninsula and the SPFA during the Early Cretaceous. This is also supported by the paleomagnetic reconstruction (Figure 7a; Beck Jr, 1999; Torsvik et al., 2012). Meanwhile, the emplacement of a syn-extensional batholith occurred along both the western margin of the SPFA and the Antarctic Peninsula at ~141–129 Ma (Figure 7a; Vaughan et al., 1998; Vaughan & Storey, 2000). Its development in Palmer Land included trench-ward migration from ~146 Ma to ~131 Ma (Figure 7a; Bastias, 2020). This magmatic event

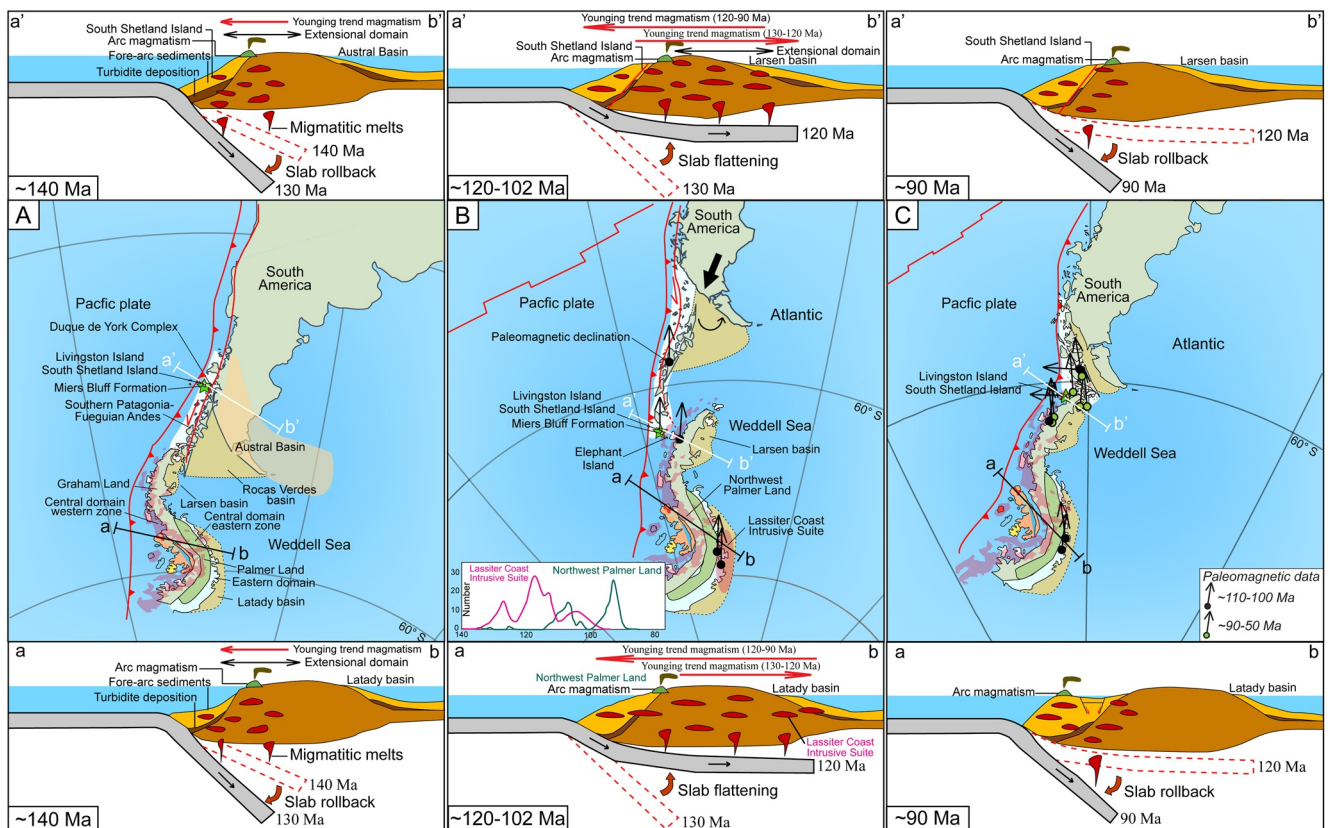


**Figure 7.** (a) Plate reconstruction of the attachment of the South Shetland Islands to the southern Patagonia-Fuegian Andes (SPFA) at ~140 Ma. The trenchward shift of magmatism occurred along the SPFA and Antarctic Peninsula at ~140–130 Ma, which was probably induced by the roll-back of the subducting Pacific Plate; (b) The South Shetland Islands experienced clockwise rotation and southward translation at ~140–120 Ma. An eastward migration of magmatism occurred from the western part to the eastern part of the Antarctic Peninsula and SPFA at ~130–120 Ma due to the slab flattening. Then, the Antarctic Peninsula experienced a westward migration of magmatism from ~120 to 90 Ma due to the roll-back of the subducting Pacific Plate. This process caused lithospheric extension and marine sediments deposition in the Larsen basin during the Cretaceous; (c) Rapid counterclockwise rotation occurred at the South Shetland Islands and SPFA from ~102 to 90 Ma but lack in the Antarctic Peninsula. At the same time, the South America experienced increased southwestward drift during the increasing seafloor spreading in the South Atlantic. The Pacific Plate subduction was limited along the Hey Cortana look transporter western margin of Antarctic Peninsula and SPFA after ~90 Ma. Cross sections of the evolution of Antarctic Peninsula were modified from Jordan et al., (2020). a–b and a'–b': Cross section line.

is akin to the first trenchward shift of magmatism along the SPFA, which was ascribed to the roll-back of the subducting Pacific Plate (Figure 7a; Guillot, 2016; Hervé et al., 2007).

Paleomagnetic data reveal that the South Shetland Islands translated southward along the Pacific margin of SPFA and experienced a clockwise rotation at ~140–120 Ma, which matches an episode of sinistral shear along the western margin of the South America, which occurred at ~139–119 Ma (Figures 7a and 7b; Seymour et al., 2020). The overlapping paleopoles indicate that South America, the SPFA, and the South Shetland Islands experienced small-scale plate motion at ~120–102 Ma (Figure 6), which is supported by analyses of absolute motion beneath the moving-hotspot reference frame (Somoza & Zaffarana, 2008).

In the Antarctic Peninsula, Early Cretaceous (~146–131 Ma) magmatism crops out primarily in western Palmer Land, with limited exposures identified from Graham Land. Whereas mid-Cretaceous magmatism is widely distributed across both Palmer Land and Graham Land in the interval, ~125–100 Ma (Figures 7a and 7b; Bastias, 2020; Riley et al., 2018, 2020). In the southeastern Antarctic Peninsula, the sedimentary succession of the Latady Basin was intruded by the enigmatic inboard arc-magmatism of the Lassiter Coast Intrusive Suite (LCIS), with three distinct magmatic peaks identified at 130–126 Ma, 118–113 Ma, and 108–102 Ma and controlled by sinistral transpression during the Palmer Land Event (Riley et al., 2016, 2018). The outcrop of the LCIS represents an eastward migration of magmatism from the western part of the Peninsula to the eastern part of the Peninsula. This was ascribed to slab flattening or secondary subduction

**Table 2**  
Cretaceous-Cenozoic Paleomagnetic Data of the South Shetland Islands, Antarctic Peninsula, and South America

Age	Sampling site	Dec	Inc	$\alpha_{95}$	Paleopole			Reference
					Lat. (S)	Long. (E)	$A_{95}$ (°)	
South Shetland Islands and Antarctic Peninsula								
140 Ma	Byers Peninsula, Livingston Island	320.1	−62.2	6.3	60.0	50.0	9.5	(1)
120 Ma	Byers Peninsula, Livingston Island	304.3	−73.2	4.2	63.4	11.4	7.1	(2)
107 Ma	Byers Peninsula, Livingston Island	298.1	−79.4	11.8	63.2	331.3	29.9	(1)
102 Ma	Byers Peninsula, Livingston Island	286.1	−75.5	3.5	58.1	354.3	6.3	This study
90 Ma	South Shetland Island and Antarctic Peninsula	359.2	−72.1	2.0	86.8	113.0	3.4	(3)
55 Ma	South Shetland Island and Antarctic Peninsula	167.1	74.0	3.4	85.0	45.5	5.6	(2)
Antarctic Peninsula								
140 Ma	Apparent Polar Wander Paths Reference site: 65.2°S, 295.9°E (Moot Point)	28.0	−68.8	3.8	70.8	176.8	6.0	(4)
100 Ma	Apparent Polar Wander Paths Reference site: 65.2°S, 295.9°E (Moot Point)	11.8	−76.5	1.9	84.9	202.0	3.3	(4)
95–110 Ma	Northern Lassiter Coast (Eastern Domain)	354.7	−80.7	3.6	88.0	62.5	6.8	(5)
95–110 Ma	Central Lassiter Coast (Eastern Domain)	0.8	−84.3	2.7	85.6	294.2	5.3	(5)
117–106 Ma	Moot Point (Central Domain)	19.0	−73.1	4.3	80.3	167.6	8.1	(1, 6)
South America								
130 Ma	–	–	–	–	84.6	65.9	1.2	(7)
125–100 Ma	Florianopolis Dykes Baqueró Group Santo Agostinho Lavas	–	–	–	88.7	354.0	2.3	(8)
85–65 Ma	Poços de Caldas Complex São Sebastião Island Passa Quatro – Itataia complexes Patagonian Basalts	–	–	–	80.6	345.1	4.3	(8)
55–40 Ma	Patagonia	–	–	–	81.0	337.4	5.7	(9)
Southern Patagonia-Fuegian Andes								
125–100 Ma	Ballenero-Obrien C.	225.7	−69.9	18.6	25.1	317.3	29.6	(10)
115–100 Ma	Hardy Pen	261.6	−72.9	4.6	41.1	335.4	7.7	(10)
90–75 Ma	Beagle-Murray Channel	316.8	−72.9	4.6	66.4	355.4	7.7	(10)
60–50 Ma	Ballenero Brecknock	320.8	−74.2	3.9	68.6	347.3	6.7	(10)

Note. References: (1) Grunow (1993); (2) Gao et al. (2018); (3) Poblete et al. (2011); (4) Torsvik et al. (2012); (5) Kellogg and Reynolds (1978); (6) Bakhmutov and Shpyra (2011); (7) Beck (1999); (8) Somoza and Zaffarana (2008); (9) Somoza (2007); (10) Poblete et al. (2016). Lat. (S): Latitude of the paleopole; Long. (E): Longitude of the paleopole;  $A_{95}$ : Radius of the 95% confidence circle about the mean paleopole position. N: Site numbers.

(Bastias, 2020; Ferraccioli et al., 2006). Spang Subduction-related epidote-amphibolite facies rocks, also developed on Elephant Island in the South Shetland Islands, at ~120–80 Ma (Dalziel, 1972a). This marks a trenchwards-younging trend of magmatism from the LCIS (eastern Palmer Land) to western Palmer Land (Riley et al., 2020) and may be a consequence of progressive roll-back of a flat-slab segment following the magmatic peak at ~118–113 Ma (Figures 7b and 7c). The subduction of oceanic crust also continued with magmatism shifting craton-ward at the SPFA after ~130 Ma (Hervé et al., 2007), which was also suggested to be caused by slab flattening (Guillot, 2016; Stern et al., 1991). Therefore, the Antarctic Peninsula and SPFA experienced a near-synchronous tectonic-magmatic history from extensive arc and back-arc tectonics during the Early Cretaceous at ~140–120 Ma, to the westward migration of magmatism at ~120–100 Ma,

during the Pacific Plate subduction (Figures 7a and 7b). The continuous magmatism and consistent Cretaceous northward paleomagnetic declination within the Central domain and the Eastern domain of the Antarctic Peninsula are consistent with the autochthonous continental subduction model (Figures 1, 7b and c; Burton-Johnson & Riley, 2015; Suárez & Pettigrew, 1976).

Our new data reveal that Byers Peninsula underwent counterclockwise rotation at ~102–90 Ma, with a Euler pole at 71.2°S, 314.6°E (Figures 5g, 6, and 7). Byers Peninsula is a part of Livingston Island, South Shetland Islands, which was considered to form part of the Western domain in the terrane accretion model of Vaughan and Storey (2000). The regular distribution of magmatic rocks from Livingston Island to King George Island suggests that there was no significant relative plate motion among these islands (Figure 1b; Haase et al., 2012; Smellie et al., 1984). Also, we exclude the local deformation induced counterclockwise rotation of Byers Peninsula within the South Shetland Islands. Because if counterclockwise rotation was induced by regional strike-slip fault movement and horizontal block rotation, we should observe the similar variation between the bedding strike and paleomagnetic declination (Milanese et al., 2020), and the fault offset during the block rotation within the South Shetland Islands. However, there is no geological evidence in support of the existence of a large-scale fault offset in Byers Peninsula or other areas within the South Shetland Islands. Paleomagnetic declination also did not change with bedding strike direction within the South Shetland Islands (Figure 1b). Therefore, we exclude the possibility of local fault strike-slip induced counterclockwise rotation between Byers Peninsula and other parts of the South Shetland Islands.

In addition, basin inversion and the closure of the Rocas Verdes Basin were initiated after the Aptian (Bruhn & Dalziel, 1977), continuing with the similar counterclockwise rotation of the Fuegian Andes from ~100 Ma to ~90 Ma (Figures 5g and 7; Somoza, 2007; Somoza & Zaffarana, 2008; Poblete et al., 2016). The paleopoles can be fitted with a small circle rotated around the northern Fuegian Andes (Figure 6a; 51.7°S, 286.1°E). Therefore, the synchronous equivalent counterclockwise rotation further supports an affinity between the South Shetland Islands and southern Patagonia-Fuegian Andes before ~90 Ma. The overlapping paleopoles between ~90–75 and ~60–50 Ma support the conclusion that the Rocas Verdes Basin was almost closed (Dalziel et al., 1974), and the cessation of tectonic rotation between the South Shetland Islands and the Antarctic Peninsula at ~90 Ma (Figure 6).

The counterclockwise rotation of the SPFA and the South Shetland Islands was contemporaneous with the increased spreading rate experienced along the South Atlantic ridge (Figure 7b; Granot & Dymont, 2015; Seton et al., 2012) and the speeding up of southwestward drift of South America from ~100 to 90 Ma (Figures 7b and 7c). Therefore, we suggest that the increased southwestward drift of South America caused counterclockwise change in the rotation of the SPFA and the South Shetland Islands, and the closure of the back-arc basin system from Rocas Verdes to northern Peru (Figures 7b and 7c; Dalziel, 1986).

In summary, the subduction related continuous magmatism and consistent, almost northward paleomagnetic declination between the Central domain and the Eastern domain support an autochthonous model in the tectonic development of the Antarctic Peninsula. Plate reconstructions also suggest that the South Shetland Islands may have originated from the Pacific margin of southern Patagonia-Fuegian Andes. The translation of the South Shetland Islands to its location adjacent to the northern Antarctic Peninsula was accomplished by a counterclockwise rotation at ~100–90 Ma. Counterclockwise rotation has been from the same period in southern Patagonia-Fuegian Andes. Therefore, the existing paleomagnetic data and geological evidence support that the Central domain and the Eastern domain were most likely formed in situ, but the South Shetland Islands of the Western domain in the northern Antarctic Peninsula may have been exotic, from the nearby proto-Pacific margin of southern Patagonia-Fuegian Andes.

## 6. Conclusions

A new mid-Cretaceous paleopole (58.1°S, 354.3°E,  $A_{95} = 6.3^\circ$ ) has been obtained from Livingston Island, South Shetland Islands of the Western domain in the northern Antarctic Peninsula. Plate reconstructions based on the paleomagnetic data are consistent with the geological evidence and support the recently proposed autochthonous model for the tectonic development of the Antarctic Peninsula (Burton-Johnson & Riley, 2015). However, plate reconstructions at ~140 Ma reveals that the South Shetland Islands may have originated from the western margin of the southern Patagonia-Fuegian Andes. The South Shetland Islands

then underwent southward translation from ~140 to ~120 Ma, which was followed by a period of small-scale plate motion at ~120–100 Ma. Lastly, a counterclockwise rotation occurred at both the South Shetland Islands and the southern Patagonia-Fuegian Andes during ~100–90 Ma as a consequence of the southwestward drift of South America. The South Shetland Islands current location adjacent to the northern Antarctic Peninsula at this period, is a result of a counterclockwise rotation.

## Data Availability Statement

The data reported in this study can be found in the Supporting Information S1 and the public repository (<https://doi.org/10.6084/m9.figshare.15153615>).

## Acknowledgments

This research was jointly funded by the Natural Science Foundation of China (NSFC) (41930218), the National Key R&D Program of China (2018YFC1406904), the National Science Foundation of China (NSFC) (42076223, 41706222), the Fundamental Research Funds for the Central Universities (35832020094), the open foundation project (KLPTR-03) of the Key Laboratory of Paleomagnetism and Tectonic Reconstruction, Ministry of Land and Resources, and the 111 project (B20011). We wish to thank the Editor Mark J. Dekkers, Associate Editor Agnes Kontny, Christine Smith Siddoway, Anne Grunow and another two anonymous reviewers for their constructive reviews of the manuscript. We are grateful for the supports from the Antarctic Administration of China, the Polar Research Institute of China and the Chinese Antarctic Great Wall Station. We sincerely thank all members of the 32nd (2015–2016), 33rd (2016–2017) Chinese National Antarctic Research Expedition, the Sino-Chilean Antarctic Expedition and the crews of *Betanzos* for their help during the fieldwork. Special thanks are due to José Retamales of the University of Magallanes, Marcelo Lepe of the Instituto Antártico Chileno (INACH) for their support during the expeditions.

## References

- Bakhmutov, V., & Shpyra, V. (2011). Palaeomagnetism of Late Cretaceous-Paleocene igneous rocks from the western part of the Antarctic Peninsula (Argentine Islands Archipelago). *Geological Quarterly*, 55(4), 285–300.
- Barbeau, D. L., Davis, J. T., Murray, K. E., Valencia, V., Gehrels, G. E., Zahid, K. M., & Gombosi, D. J. (2010). Detrital-zircon geochronology of the metasedimentary rocks of north-western Graham Land. *Antarctic Science*, 22(1), 65–78. <https://doi.org/10.1017/S095410200999054X>
- Bastias, J. (2020). *The Triassic-Cretaceous tectonomagmatic history of the Antarctic Peninsula constrained by geochronology, thermochronology and isotope geochemistry* (Doctoral dissertation). University of Geneva.
- Bastias, J., Calderón, M., Israel, L., Hervé, F., Spikings, R., Pankhurst, R., et al. (2019). The Byers Basin: Jurassic-Cretaceous tectonic and depositional evolution of the forearc deposits of the South Shetland Islands and its implications for the northern Antarctic Peninsula. *International Geology Review*, 62, 1–1484. <https://doi.org/10.1080/00206814.2019.1655669>
- Beck, M. E., Jr. (1999). Jurassic and Cretaceous apparent polar wander relative to South America: Some tectonic implications. *Journal of Geophysical Research*, 104(B3), 5063–5067. <https://doi.org/10.1029/98JB02839>
- Blundell, D. J. (1962). Palcomagnetic investigation in the Falkland Island Dependencies. *British Antarctic Survey Scientific Reports*, 12, 39.
- Boyden, J. A., Müller, R. D., Gurnis, M., Torsvik, T. H., Clark, J. A., Turner, M., et al. (2011). Next-generation plate-tectonic reconstructions using GPlates. In G. R. Keller, & C. Baru (Eds.), *Geoinformatics: Cyberinfrastructure for the Solid earth sciences* (pp. 95–113). Cambridge University Press.
- Bruhn, R. L., & Dalziel, I. W. D. (1977). Destruction of the Early Cretaceous marginal basin in the Andes of Tierra del Fuego: Island Arcs. *Deep Sea Trenches and Back-Arc Basins*, 1, 395–405. <https://doi.org/10.1029/me001p0395>
- Burton-Johnson, A., & Riley, T. R. (2015). Autochthonous v. accreted terrane development of continental margins: A revised in situ tectonic history of the Antarctic Peninsula. *Journal of the Geological Society*, 172(6), 822–835. <https://doi.org/10.1144/jgs2014-110>
- Butler, R. F. (1998). *Paleomagnetism: Magnetic domains to geologic terranes* (Electronic ed., p. 238). Department of Geosciences.
- Castillo, P., Fanning, C. M., Hervé, F., & Lacassie, J. P. (2016). Characterisation and tracing of Permian magmatism in the south-western segment of the Gondwana margin: U-Pb age, Lu-Hf and O isotopic compositions of detrital zircons from metasedimentary complexes of northern Antarctic Peninsula and western Patagonia. *Gondwana Research*, 36, 1–13. <https://doi.org/10.1016/j.gr.2015.07.014>
- Cisowski, S. M., Dunn, J. R., Fuller, M., & Wasilewski, P. J. (1990). NRM: IRM (s) demagnetization plots of intrusive rocks and the origin of their NRM. *Tectonophysics*, 184(1), 35–54. [https://doi.org/10.1016/0040-1951\(90\)90119-5](https://doi.org/10.1016/0040-1951(90)90119-5)
- Cogné, J. P. (2003). PaleoMac: A Macintosh™ application for treating paleomagnetic data and making plate reconstructions. *Geochemistry, Geophysics, Geosystems*, 4(1). <https://doi.org/10.1029/2001GC000227>
- Compston, W., Williams, I. S., Kirschvink, J. L., Zichao, Z., & Guogan, M. (1992). Zircon U-Pb ages for the Early Cambrian time-scale. *Journal of the Geological Society*, 149(2), 171–184. <https://doi.org/10.1144/gsjgs.149.2.0171>
- Dalziel, I. W. D. (1972a). K-Ar dating of rocks from Elephant Island, south Scotia Ridge. *The Geological Society of America Bulletin*, 83(6), 1887–1894. [https://doi.org/10.1130/0016-7606\(1972\)83\[1887:KDORFE\]2.0.CO;2](https://doi.org/10.1130/0016-7606(1972)83[1887:KDORFE]2.0.CO;2)
- Dalziel, I. W. D. (1972b). Large scale folding in the Scotia Arc. In R. J. Adie (Ed.), *Antarctic geology and geophysics* (pp. 47–55). Universitetsforlaget.
- Dalziel, I. W. D. (1986). Collision and Cordilleran orogenesis: An Andean perspective. *Geological Society, London, Special Publications*, 19(1), 389–404. <https://doi.org/10.1144/GSL.SP.1986.019.01.22>
- Dalziel, I. W. D., de Wit, M. J., & Palmer, K. F. (1974). Fossil marginal basin in the southern Andes. *Nature*, 250(5464), 291–294. <https://doi.org/10.1038/250291a0>
- Dalziel, I. W. D., & Elliot, D. H. (1971). Evolution of the Scotia arc. *Nature*, 233(5317), 246–252. <https://doi.org/10.1038/233246a0>
- Dalziel, I. W. D., & Elliot, D. H. (1982). West Antarctica: Problem child of Gondwanaland. *Tectonics*, 1(1), 3–19. <https://doi.org/10.1029/TC001i001p00003>
- Dalziel, I. W. D., Kligfield, R., Lowrie, W., & Opdyke, N. D. (1973). Paleomagnetic Data from the Southernmost Andes and the Antartandes. In *Implications of Continental Drift to the Earth Sciences* (Vol. 1, pp. 87–101). Academic Press.
- Deenen, M. H., Langereis, C. G., van Hinsbergen, D. J. J., & Biggin, A. J. (2011). Geomagnetic secular variation and the statistics of palaeomagnetic directions. *Geophysical Journal International*, 186(2), 509–520. <https://doi.org/10.1111/j.1365-246X.2011.05050.x>
- Dunlop, D. J., & Özdemir, Ö. (2001). *Rock magnetism: Fundamentals and frontiers*. Cambridge University Press.
- Enkin, R. J. (1994). *A computer program package for analysis and presentation of paleomagnetic data* (Vol. 16). Pacific Geoscience Centre, Geological Survey of Canada.
- Enkin, R. J. (2003). The direction–correction tilt test: An all-purpose tilt/fold test for paleomagnetic studies. *Earth and Planetary Science Letters*, 212(1–2), 151–166. [https://doi.org/10.1016/S0012-821X\(03\)00238-3](https://doi.org/10.1016/S0012-821X(03)00238-3)
- Ferraccioli, F., Jones, P. C., Vaughan, A. P. M., & Leat, P. T. (2006). New aerogeophysical view of the Antarctic Peninsula: More pieces, less puzzle. *Geophysical Research Letters*, 33(5). <https://doi.org/10.1029/2005GL024636>
- Fisher, R. A. (1953). Dispersion on a sphere. *Proceedings of the Royal Society A: Mathematical, Physical and Engineering Sciences*, 217, 295–305. <https://doi.org/10.1098/rspa.1953.0064>

- Gao, L., Zhao, Y., Yang, Z. Y., Liu, J. M., Liu, X. C., Zhang, S. H., & Pei, J. L. (2018). New paleomagnetic and  $^{40}\text{Ar}/^{39}\text{Ar}$  geochronological results for the South Shetland Islands, West Antarctica, and their tectonic implications. *Journal of Geophysical Research: Solid Earth*, 123(1), 4–30. <https://doi.org/10.1002/2017JB014677>
- Gracanic, T. M. (1983). *Geochemistry and geochronology of some Mesozoic igneous rocks from the northern Antarctic Peninsula region* (unpublished MSc thesis). Ohio State University.
- Granot, R., & Dymant, J. (2015). The Cretaceous opening of the South Atlantic Ocean. *Earth and Planetary Science Letters*, 414, 156–163. <https://doi.org/10.1016/j.epsl.2015.01.015>
- Grunow, A. M. (1993). New paleomagnetic data from the Antarctic Peninsula and their tectonic implications. *Journal of Geophysical Research*, 98(B8), 13815–13833. <https://doi.org/10.1029/93JB01089>
- Guillot, M. G. (2016). Magmatic evolution of the southernmost Andes and its relation with subduction processes. In *Geodynamic evolution of the Southernmost Andes* (pp. 37–74). Springer. [https://doi.org/10.1007/978-3-319-39727-6\\_3](https://doi.org/10.1007/978-3-319-39727-6_3)
- Haase, K. M., Beier, C., Fretzdorff, S., Smellie, J. L., & Garbe-Schönberg, D. (2012). Magmatic evolution of the South Shetland Islands, Antarctica, and implications for continental crust formation. *Contributions to Mineralogy and Petrology*, 163(6), 1103–1119. <https://doi.org/10.1007/s00410-012-0719-7>
- Harrison, R. J., & Feinberg, J. M. (2008). FORCinel: An improved algorithm for calculating first-order reversal curve distributions using locally weighted regression smoothing. *Geochemistry, Geophysics, Geosystems*, 9. <https://doi.org/10.1029/2008GC001987>
- Hathway, B. (2000). Continental rift to back-arc basin: Jurassic–Cretaceous stratigraphical and structural evolution of the Larsen Basin, Antarctic Peninsula. *Journal of the Geological Society*, 157(2), 417–432. <https://doi.org/10.1144/jgs.157.2.417>
- Hathway, B., Duane, A. M., Cantrill, D. J., & Kelley, S. P. (1999).  $^{40}\text{Ar}/^{39}\text{Ar}$  geochronology and palynology of the Cerro Negro Formation, South Shetland Islands, Antarctica: A new radiometric tie for Cretaceous terrestrial biostratigraphy in the Southern Hemisphere. *Australian Journal of Earth Sciences*, 46(4), 593–606. <https://doi.org/10.1046/j.1440-0952.1999.00727.x>
- Hathway, B., & Lomas, S. A. (1998). The upper Jurassic–Lower Cretaceous Byers Group, South Shetland Islands, Antarctica: Revised stratigraphy and regional correlations. *Cretaceous Research*, 19, 43–67. <https://doi.org/10.1006/cres.1997.0095>
- Hervé, F., Faúndez, V., Brix, M., & Fanning, M. (2006). Jurassic sedimentation of the Miers Bluff Formation, Livingston Island, Antarctica: Evidence from SHRIMP U–Pb ages of detrital and plutonic zircons. *Antarctic Science*, 18(2), 229–238. <https://doi.org/10.1017/S0954102006000277>
- Hervé, F., Miller, H., & Pimpirev, C. (2006). *Patagonia–Antarctica connections before Gondwana break-up: In Antarctica* (pp. 217–227). Springer. [https://doi.org/10.1007/3-540-32934-X\\_26](https://doi.org/10.1007/3-540-32934-X_26)
- Hervé, F., Pankhurst, R. J., Fanning, C. M., Calderón, M., & Yaxley, G. M. (2007). The South Patagonian batholith: 150 my of granite magmatism on a plate margin. *Lithos*, 97(3–4), 373–394. <https://doi.org/10.1016/j.lithos.2007.01.007>
- Hobbs, G. J. (1968). *The geology of The south Shetland islands: IV. The geology of Livingston Island*.
- Holdsworth, B. K., & Nell, P. A. R. (1992). Mesozoic radiolarian faunas from the Antarctic Peninsula: Age, tectonic and palaeoceanographic significance. *Journal of the Geological Society*, 149(6), 1003–1020. <https://doi.org/10.1144/gsjgs.149.6.1003>
- Hrouda, F. (1982). Magnetic anisotropy of rocks and its application in geology and geophysics. *Geophysical Surveys*, 5(1), 37–82. <https://doi.org/10.1007/BF01450244>
- Hunter, M. A., & Cantrill, D. J. (2006). A new stratigraphy for the Latady Basin, Antarctic Peninsula: Part 2, Latady Group and basin evolution. *Geological Magazine*, 143(6), 797–819. <https://doi.org/10.1017/S0016756806002603>
- Jordan, T. A., Ferraccioli, F., & Leat, P. T. (2017). New geophysical compilations link crustal block motion to Jurassic extension and strike-slip faulting in the Weddell Sea Rift System of West Antarctica. *Gondwana Research*, 42, 29–48. <https://doi.org/10.1016/j.gr.2016.09.009>
- Jordan, T. A., Neale, R. F., Leat, P. T., Vaughan, A. P. M., Flowerdew, M. J., Riley, T. R., et al. (2014). Structure and evolution of Cenozoic arc magmatism on the Antarctic Peninsula: A high resolution aeromagnetic perspective. *Geophysical Journal International*, 198(3), 1758–1774. <https://doi.org/10.1093/gji/ggu233>
- Jordan, T. A., Riley, T. R., & Siddoway, C. S. (2020). The geological history and evolution of West Antarctica. *Nature Reviews Earth & Environment*, 1, 1–133. <https://doi.org/10.1038/s43017-019-0013-6>
- Kellogg, K. S., & Reynolds, R. L. (1978). Paleomagnetic results from the Lassiter Coast, Antarctica, and a test for oroclinal bending of the Antarctic Peninsula. *Journal of Geophysical Research*, 83(B5), 2293–2299. <https://doi.org/10.1029/JB083iB05p02293>
- Kellogg, K. S., & Rowley, P. D. (1989). *Structural geology and tectonics of the Orville Coast region, southern Antarctic Peninsula, Antarctica*. United States Geological Survey, Professional Paper (USA).
- Kirschvink, J. L. (1980). The least-squares line and plane and the analysis of palaeomagnetic data. *Geophysical Journal International*, 62(3), 699–718. <https://doi.org/10.1111/j.1365-246X.1980.tb02601.x>
- Leat, P. T., & Riley, T. R. (2021). *A Antarctic Peninsula and South Shetland Islands: Volcanology* (Vol. 55). Geological Society. <https://doi.org/10.1144/m55-2018-52>
- Leat, P. T., Scarrow, J. H., & Millar, I. L. (1995). On the Antarctic Peninsula batholith. *Geological Magazine*, 132(4), 399–412. <https://doi.org/10.1017/S0016756800021464>
- Ludwig, K. R. (2003). Isoplot 3.00. In *A Geochronological Toolkit for Microsoft Excel* (Vol. 4, p. 70). Berkeley Geochronology Center Special Publication.
- Milanese, F. N., Rapalini, A., Gallo, L., Franceschini, P., & Kirschvink, J. (2020). Large paleomagnetic declination anomalies in the Cerro Nevado (Snow Hill) Island, Antarctic Peninsula: Evidence of hidden tectonic rotations? *Revista de la Asociación Geológica Argentina*, 77(2), 192–206.
- Milanese, F. N., Rapalini, A. E., Slotznick, S. P., Tobin, T. S., Kirschvink, J. L., & Olivero, E. B. (2019). Late Cretaceous paleogeography of the Antarctic Peninsula: New paleomagnetic pole from the James Ross Basin. *Journal of South American Earth Sciences*, 91, 131–143. <https://doi.org/10.1016/j.jsames.2019.01.012>
- Müller, R. D., Cannon, J., Qin, X., Watson, R. J., Gurnis, M., Williams, S., et al. (2018). GPlates: Building a virtual Earth through deep time. *Geochemistry, Geophysics, Geosystems*, 19, 2243–2261. <https://doi.org/10.1029/2018GC007584>
- Muñoz, A., Sàbat, F., & Pallàs, R. (1992). Estructura pre-Cretácica de la Península Hurd, Isla Livingston, Islas Shetland del Sur. In J. López-Martínez (Ed.), *Geología de la Antártida Occidental. Simposios T3. III Congreso Geológico de España y VIII Congreso Latinoamericano de Geología* (pp. 127–139).
- Ogg, J. G. (2020). Geomagnetic polarity time scale. In *Geologic time scale 2020* (pp. 159–192). Elsevier. <https://doi.org/10.1016/b978-0-12-824360-2.00005-x>
- Pallàs, R., Zheng, X., Tuset, J. M. C., Montserrat, F. S., & Torrente, D. G. (1999). Mesozoic geology of Cape Shirreff, Livingston Island, South Shetland Islands, Antarctica. *Acta geológica hispánica*, 329–337.

- Pimpirev, C., Ivanov, M., Dimov, D., & Nikolov, T. (2002). First find of the Upper Tithonian ammonite genus *Blanfordiceras* from the Miers Bluff Formation, Livingston Island, South Shetland Islands. *Neues Jahrbuch für Geologie und Paläontologie - Monatshefte*, 2002, 377–384. <https://doi.org/10.1127/njgpm/2002/2002/377>
- Pimpirev, C., Stoykova, K., Ivanov, M., & Dimov, V. (2006). The Miers Bluff Formation, Livingston Island, South Shetland Islands-part of the Late Jurassic-Cretaceous depositional history of the Antarctic Peninsula. In D. K. Futterer, D. Damaske, G. Kleinschmidt, H. Miller, & F. Tessensohn (Eds.), *Antarctica: Contributions to global earth sciences* (pp. 249–254). Springer.
- Poblete, F., Arriagada, C., Roperch, P., Astudillo, N., Hervé, F., Kraus, S., & Le Roux, J. P. (2011). Paleomagnetism and tectonics of the South Shetland Islands and the northern Antarctic Peninsula. *Earth and Planetary Science Letters*, 302(3–4), 299–313. <https://doi.org/10.1016/j.epsl.2010.12.019>
- Poblete, F., Roperch, P., Arriagada, C., Ruffet, G., de Arellano, C. R., Hervé, F., & Poujol, M. (2016). Late Cretaceous-early Eocene counter-clockwise rotation of the Southern Patagonian Andes and evolution of the Patagonia-Antarctic Peninsula system. *Tectonophysics*, 668, 15–34. <https://doi.org/10.1016/j.tecto.2015.11.025>
- Riley, T. R., Burton-Johnson, A., Flowerdew, M. J., & Whitehouse, M. J. (2018). Episodicity within a mid-Cretaceous magmatic flare-up in West Antarctica: U-Pb ages of the Lassiter Coast intrusive suite, Antarctic Peninsula, and correlations along the Gondwana margin. *Bulletin*, 130(7–8), 1177–1196. <https://doi.org/10.1130/B31800.1>
- Riley, T. R., Carter, A., Leat, P. T., Burton-Johnson, A., Bastias, J., Spikings, R. A., et al. (2019). Geochronology and geochemistry of the northern Scotia Sea: A revised interpretation of the North and West Scotia ridge junction. *Earth and Planetary Science Letters*, 518, 136–147. <https://doi.org/10.1016/j.epsl.2019.04.031>
- Riley, T. R., Flowerdew, M. J., Burton-Johnson, A., Leat, P. T., Millar, I. L., & Whitehouse, M. J. (2020). Cretaceous arc volcanism of Palmer Land, Antarctic Peninsula: Zircon U-Pb geochronology, geochemistry, distribution and field relationships. *Journal of Volcanology and Geothermal Research*, 401, 106969. <https://doi.org/10.1016/j.jvolgeores.2020.106969>
- Riley, T. R., Flowerdew, M. J., Curtis, M. L., & Whitehouse, M. J. (2016). Evolution of the Antarctic Peninsula lithosphere: Evidence from Mesozoic mafic rocks. *Lithos*, 244, 59–73. <https://doi.org/10.1016/j.lithos.2015.11.037>
- Riley, T. R., Flowerdew, M. J., & Whitehouse, M. J. (2012). Chrono- and lithostratigraphy of a Mesozoic-Tertiary fore- to intra-arc basin: Adelaide Island, Antarctic Peninsula. *Geological Magazine*, 149(5), 768–782. <https://doi.org/10.1017/S0016756811001002>
- Roberts, A. P., Pike, C. R., & Verosub, K. L. (2000). First-order reversal curve diagrams: A new tool for characterizing the magnetic properties of natural samples. *Journal of Geophysical Research*, 105(B12), 28461–28475. <https://doi.org/10.1029/2000JB900326>
- Seton, M., Müller, R. D., Zahirovic, S., Gaina, C., Torsvik, T., Shephard, G., et al. (2012). Global continental and ocean basin reconstructions since 200Ma. *Earth-Science Reviews*, 113(3), 212–270. <https://doi.org/10.1016/j.earscirev.2012.03.002>
- Seymour, N. M., Singleton, J. S., Mavor, S. P., Gomila, R., Stockli, D. F., Heuser, G., & Arancibia, G. (2020). The relationship between magmatism and deformation along the intra-arc strike-slip Atacama fault system, northern Chile. *Tectonics*, 39(3), e2019TC005702. <https://doi.org/10.1029/2019TC005702>
- Smellie, J. L. (1981). A complete arc-trench system recognized in Gondwana sequences of the Antarctic Peninsula region. *Geological Magazine*, 118(2), 139–159. <https://doi.org/10.1017/S001675680003435X>
- Smellie, J. L., Davies, R. E. S., & Thomson, M. R. A. (1980). Geology of a Mesozoic intra-arc sequence on Byers Peninsula, Livingston Island, South Shetland Islands. *British Antarctic Survey Bulletin*, 50, 55–76.
- Smellie, J. L., & Hole, M. J. (2021). *A Antarctic Peninsula: Volcanology* (Vol. 55). Geological Society. <https://doi.org/10.1144/m55-2018-59>
- Smellie, J. L., Pankhurst, R. J., Thomson, M. R. A., & Davies, R. E. S. (1984). The geology of the South Shetland Islands: VI. Stratigraphy, geochemistry and evolution. *British Antarctic Survey Scientific Reports*, 87.
- Somoza, R. (2007). Eocene paleomagnetic pole for South America: Northward continental motion in the Cenozoic, opening of Drake Passage and Caribbean convergence. *Journal of Geophysical Research*, 112(B3). <https://doi.org/10.1029/2006JB004610>
- Somoza, R., & Zaffarana, C. B. (2008). Mid-Cretaceous polar standstill of South America, motion of the Atlantic hotspots and the birth of the Andean cordillera. *Earth and Planetary Science Letters*, 271(1–4), 267–277. <https://doi.org/10.1016/j.epsl.2008.04.004>
- Stern, C. R., Mohseni, P. P., & Fuenzalida, P. R. (1991). Petrochemistry and tectonic significance of lower Cretaceous Barros Arana Formation basalts, southernmost Chilean Andes. *Journal of South American Earth Sciences*, 4(4), 331–342. [https://doi.org/10.1016/0895-9811\(91\)90005-6](https://doi.org/10.1016/0895-9811(91)90005-6)
- Suárez, M., & Pettigrew, T. H. (1976). An Upper Mesozoic island-arc-back-arc system in the southern Andes and South Georgia. *Geological Magazine*, 113, 305–328. <https://doi.org/10.1017/S0016756800047592>
- Tanner, P. W. G., Pankhurst, R. J., & Hyden, G. (1982). Radiometric evidence for the age of the subduction complex in the South Orkney and South Shetland Islands, West Antarctica. *Journal of the Geological Society*, 139(6), 683–690. <https://doi.org/10.1144/gsjgs.139.6.0683>
- Thébault, E., Finlay, C. C., Beggan, C. D., Alken, P., Aubert, J., Barrois, O., et al. (2015). International Geomagnetic Reference Field: The 12th generation. *Earth Planets and Space*, 67(79). <https://doi.org/10.1186/s40623-015-0228-9>
- Tobin, T. S., Ward, P. D., Steig, E. J., Olivero, E. B., Hilburn, I. A., Mitchell, R. N., et al. (2012). Extinction patterns,  $\delta^{18}\text{O}$  trends, and magnetostratigraphy from a southern high-latitude Cretaceous-Paleogene section: Links with Deccan volcanism. *Palaeogeography, Palaeoclimatology, Palaeoecology*, 350–352, 180–188. <https://doi.org/10.1016/j.palaeo.2012.06.029>
- Torsvik, T. H., Van der Voo, R., Preeden, U., Mac Niocaill, C., Steinberger, B., Doubrovine, P. V., et al. (2012). Phanerozoic polar wander, palaeogeography and dynamics. *Earth-Science Reviews*, 114(3–4), 325–368. <https://doi.org/10.1016/j.earscirev.2012.06.007>
- Trouw, R. A., Passchier, C. W., Valeriano, C. M., Simões, L. S. A., Paciullo, F. V., & Ribeiro, A. (2000). Deformational evolution of a Cretaceous subduction complex: Elephant Island, South Shetland Islands, Antarctica. *Tectonophysics*, 319(2), 93–110. [https://doi.org/10.1016/S0040-1951\(00\)00021-4](https://doi.org/10.1016/S0040-1951(00)00021-4)
- Vaughan, A. P. M., Kelley, S. P., & Storey, B. C. (2002). Mid-Cretaceous ductile deformation on the Eastern Palmer Land Shear Zone, Antarctica, and implications for timing of Mesozoic terrane collision. *Geological Magazine*, 139, 46–471. <https://doi.org/10.1017/S0016756802006672>
- Vaughan, A. P. M., Pankhurst, R. J., & Fanning, C. M. (2002). A mid-Cretaceous age for the Palmer Land event, Antarctic Peninsula: Implications for terrane accretion timing and Gondwana palaeolatitudes. *Journal of the Geological Society*, 159, 113–116. <https://doi.org/10.1144/0016-764901-090>
- Vaughan, A. P. M., & Storey, B. C. (2000). The eastern Palmer Land shear zone: A new terrane accretion model for the Mesozoic development of the Antarctic Peninsula. *Journal of the Geological Society*, 157(6), 1243–1256. <https://doi.org/10.1144/jgs.157.6.1243>
- Vaughan, A. P. M., Wareham, C. D., Johnson, A. C., & Kelley, S. P. (1998). A Lower Cretaceous, syn-extensional magmatic source for a linear belt of positive magnetic anomalies: The Pacific Margin Anomaly (PMA), western Palmer Land, Antarctica. *Earth and Planetary Science Letters*, 158(3–4), 143–155. [https://doi.org/10.1016/S0012-821X\(98\)00054-5](https://doi.org/10.1016/S0012-821X(98)00054-5)

- Wareham, C. D., Millar, I. L., & Vaughan, A. P. (1997). The generation of sodic granite magmas, western Palmer Land, Antarctic Peninsula. *Contributions to Mineralogy and Petrology*, 128(1), 81–96. <https://doi.org/10.1007/s004100050295>
- Watson, G. S., & Enkin, R. J. (1993). The fold test in paleomagnetism as a parameter estimation problem. *Geophysical Research Letters*, 20(19), 2135–2137. <https://doi.org/10.1029/93GL01901>
- Watts, D. R., Watts, G. C., & Bramall, A. M. (1984). Cretaceous and early Tertiary paleomagnetic results from the Antarctic Peninsula. *Tectonics*, 3(3), 333–346. <https://doi.org/10.1029/TC003i003p00333>
- Zheng, G. G., Liu, X. C., Liu, S. W., Zhang, S. H., & Zhao, Y. (2018). Late Mesozoic–early Cenozoic intermediate–acid intrusive rocks from the Gerlache Strait area, Antarctic Peninsula: Zircon U–Pb geochronology, petrogenesis and tectonic implications. *Lithos*, 312, 204–222. <https://doi.org/10.1016/j.lithos.2018.05.008>